Defence Science Journal, Vol. 74, No. 6, November 2024, pp. 777-786, DOI : 10.14429/dsj.74.19119

Effect of Variation of Damping Gap on Damping and Unbalance Response of a Compact Squeeze Film Damper: Experiments and Simulations

Anurag Kumar[*], Aman K. Srivastava, Mayank Tiwari, and Akhilendra Singh

Indian Institute of Technology, Patna - 801 106, India
[*]E-mail: anurag.pme17@iitp.ac.in

ABSTRACT

Squeeze Film Dampers play a crucial role in rotating machinery by effectively dampening vibration amplitudes. As a result, various designs of SFDs have been developed for widespread industrial applications. The current investigation introduces a design for a Compact Squeeze Film Damper (CSFD), drawing inspiration from the ISFD design. Parameters such as the damping coefficient of the CSFD are determined through Finite Element simulation Method (FEM) and experimental techniques. The fabrication and integration of the compact squeeze film damper with a rotor rig are executed, followed by the presentation of rotor responses across various frequencies. The study delves into the impact of CSFD geometry, particularly clearance and length, on the damping performance of the CSFD. Orbit plots vividly illustrate the Compact squeeze film damper's ability to reduce rotor vibration amplitudes. Frequency spectra generated from FEM data reveal the nonlinear behaviour of the CSFD, characterized by the presence of odd harmonics, while experimental results exhibit the presence of both odd and even harmonics. Response plots demonstrate a softening effect on the rotor within the rotor-CSFD system. Investigating the geometric parameters of compact squeeze film damper unveils an inverse relationship between Compact squeeze film damper clearance and damping ratio. Moreover, an increase in the length of Compact squeeze film damper correlates with a higher damping ratio. The modified Rayleigh oscillator studied in this paper has similar frequencies and orbit response as observed from compact squeeze film damper. This hints towards the presence of cubic damping similar to the rayleigh oscillator in the proposed compact squeeze film damper.

Keywords: Compact squeeze film damper; Nonlinear behaviour; Orbit plot; Finite element simulation method

1. INTRODUCTION

The Squeeze Film Damper (SFD) is employed to dampen the vibration response of rotors in rotating machinery. Due to the presence of fluid as the working medium, its behaviour exhibits nonlinearity. Numerous studies have been conducted in the field of SFD design in rotor systems[1-2], including analyses of the nonlinear response of concentric and eccentric SFDs[3]. Yakoub and El-Shafei[4-5] utilised a planar modal analysis approach to acquire the unbalanced (nonlinear) response of multi-mode rotors supported by SFDs and conducted a parametric investigation to design SFDs for aircraft gas turbine fans. Chen and Hahn[6] examined the influence of end seal clearance and flow path length on the performance of centrally orbiting SFDs with a circumferential groove at the centre using computational fluid dynamics (CFD). Bonello[7], *et al.* investigated the nonlinear dynamics of rotor systems supported by SFDs with and without retainer springs. Bao[8], *et al.* investigated the damping characteristics of squeeze film air damping in perforated structures. Xing[9-10], *et al.* conducted an analysis of pressure distribution, damping coefficient, and rotor system stability in the presence of homogeneous gaseous cavitation in SFDs. Locke and Faller[11] utilised an innovative Integral Squeeze Film Damper (ISFD) to address the issue of compressor imbalance resulting from impeller erosion. De Santiago and San Andres[12-15] carried out comprehensive laboratory experiments on both open-ended and end-sealed ISFDs. They determined force coefficients through component impact tests and investigated the influence of imbalance on vibration response. Childs and Agnew[16] conducted component tests on flexure pivot bearings supported by ISFDs, calculating force coefficients for both active and locked ISFD configurations. Their results reveal that the force coefficient of the active damper is 50 % less stiff than that of the locked damper, while damping shows a modest decrease. Ertas Burga[17], *et al.* utilised ISFD to stabilize the sub-synchronous response of a 46 MW steam turbine. Their observations revealed a significant improvement in stability margin by a factor of 12, eliminating sub-synchronous instability and markedly reducing the critical speed amplification factor. In another study, Ertas[18], *et al.* employed experimental and analytical methods to determine the stiffness and damping coefficients of ISFD across various end seal gap widths, vibration frequencies, and amplitudes. The research demonstrated consistent damping behaviour for each end seal gap until cavitation or air ingestion occurred, with the direct stiffness exhibiting linearity. Finite element analysis was employed to solve the modified Reynolds equation to visualize the effect of added fluid inertia on ISFD, with the prediction and experimental results showing a good

Received : 26 May 2023, Revised : 18 March 2024
Accepted : 06 June 2024, Online published : 25 November 2024

correlation for direct damping. However, the prediction of the inertia coefficient was found to be overestimated compared to the experimental results. Xueliang Lu[19], *et al.* investigated the impact of the end seal gap on the dynamic force coefficient of ISFD through experimental and predictive methods. Their findings indicated that ISFDs with tighter end seals exhibited nearly 20 times more damping than open-end ISFDs, although this configuration also displayed stiffness hardening with increasing excitation frequency. Furthermore, ISFDs with loose-end seals accurately predicted the damping coefficient, while the added mass coefficient was underestimated.

The literature review highlights a prevalent focus on ISFDs combined with tilting pads in previous studies. This study introduces a novel design of CSFD equipped with integrated M-shaped springs, offering both stiffness and damping improvements over conventional SFDs. Inspired by the ISFD® design, this approach does not include tilting pads, making it suitable for retrofitting applications. The primary objective of this study is to characterize the parameters of CSFD, such as stiffness and damping, using a combination of experimental and simulation techniques.

2. SIMULATION AND EXPERIMENTAL METHODS

2.1 Design of Proposed Compact Squeeze Film Damper

The proposed CSFD studied in this work is manufactured by wire electric discharge machining process (WEDM) and is shown in Fig. 1(a). The CSFD is mainly divided into four parts: inner rim, outer rim, integral springs and damping land. The outer rim is fitted and fixed to the bearing housing. The inner rim fits snugly against the outer race of the rolling bearing. The outer diameter of CSFD is 75 mm, and the inner diameter is 47 mm. The damping land gap (c) is machined at a radius of 30.1mm. The integral M-shape springs provide stiffness to the system. The proposed CSFD is covered from both sides by the end-plate, which is assembled by four Allen screws. Oil is filled inside the damper by an external pump through the hole made on the face of the end plate. The oil exhibits a dynamic viscosity of 0.0312 Pa-s and a density of 850 kg/m³. The cross-sectional view of the CSFD covered with end plates from both sides is shown in Fig. 1(c), and the exploded view of the CSFD assembly is shown in Fig. 1(b).

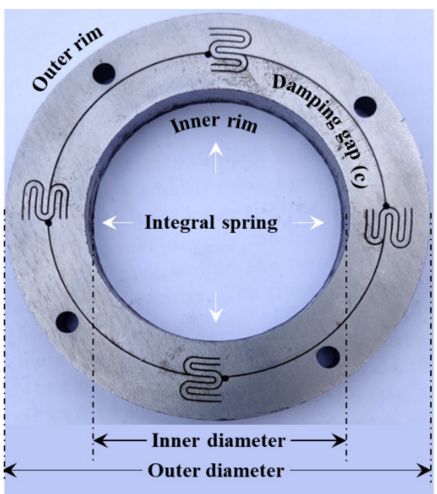

(a)

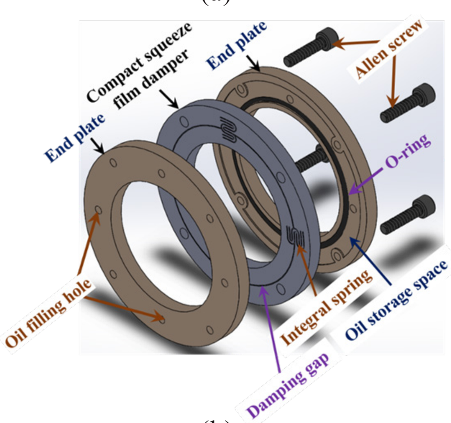

(b)

Figure 1. (a) Drawing of the compact squeeze film damper, and (b) Exploded view of CSFD assembly.

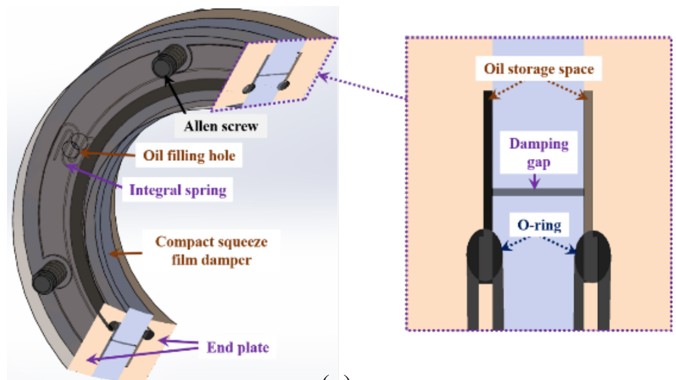

(c)

Figure 1. (c) Cross-sectional view of Compact squeeze film damper covered with end-plates.

2.2 FEM Analysis of Compact Squeeze Film Damper

Finite element analysis of CSFD has been carried out using ANSYS 19.1© (Academic license). This section provides a comprehensive algorithm for FEM solution, i.e. pre-processing, solution and post-processing, applied to the CSFD. The pre-processing phase involves the development of a generalized APDL code to create the CSFD model, apply boundary conditions, and impose the unbalance load. This includes the creation of a 3-dimensional model of the CSFD, with the solid part of the damper discretized using an 8-node 3D solid element capable of displacement in all three directions.

Additionally, fluid elements governed by the nonlinear Reynolds equation are utilised, each consisting of 4 nodes with 4° of freedom (displacements and pressure), to represent the fluid behaviour within the damper. These fluid elements are employed to calculate the pressure distribution within the squeeze film damper based on the instantaneous shaft position. Furthermore, the outer diameter of the CSFD's outer rim is constrained in all degrees of freedom, while the inner diameter of the inner rim is rigidly supported to transfer the unbalance load. Finally, a rotating unbalance force of 10 N is applied at the centre of the rigid constraint. Throughout the solution phase, a comprehensive transient, nonlinear approach was utilised. The solution was executed for 1 sec, employing a time step size of 0.00001 and a solution tolerance of 1.0^{-10}. Following the completion of the solution phase, post-processing activities were conducted to extract pertinent results, including damping force and shaft displacement, for subsequent analysis.

2.3 Experimental Test Rig Description

Figure 2 shows the experimental rig (setup on basic Gunt© GmbH Machinery Diagnostic system) used for the present study. The test setup consists of a 500 mm long and 10 mm diameter shaft stepped at both ends for bearing support with a step diameter of 20 mm. A disc of 10 mm thickness and 140mm diameter is shrink-fitted at the middle span of the shaft. The shaft is supported by a normal ball bearing from the driving end and a ball bearing attached to the CSFD at the free end. The rotor is coupled with a 3-phase 6000 rpm motor by elastic claw coupling. Two proximity probes are attached at orthogonal position, one in the vertical (y) direction (at the top of the shaft) and the other in the horizontal (x) direction, to capture the whirling motion of the shaft. The 1st natural frequency of the test rig used for the experiment shown in Fig. 2 is 37.5 Hz, which has been obtained through the modal test. National Instruments (NI) cDAQ-9185 chassis and NI-9234 module have been used to acquire and store the vibration data.

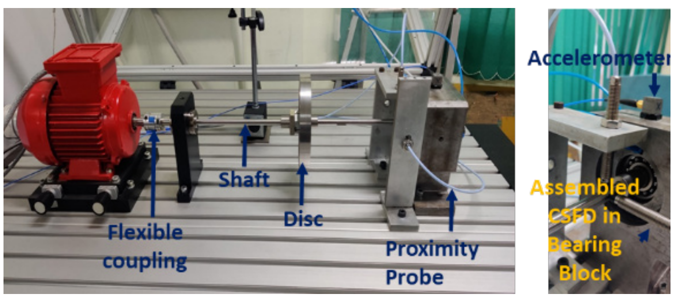

Figure 2. Arrangement of the experimental setup.

3. RESULTS AND DISCUSSIONS

3.1 Damping Coefficient From Fem Analysis

A parametric investigation was conducted to analyze the variation of the damping coefficient with the axial length (L) and damping gap (c) of CSFD, as outlined in the experimental design presented in Table 1. Each configuration of Table 1 represents a specific combination of parameters, such as clearance and axial length, in the CSFD design. These configurations are essential for studying the effects of these parameters on the damping behaviour of the damper. By investigating multiple configurations, we can determine the optimal combination of parameters to achieve desired damping performance.

Figure 3(a) illustrates the trend of the damping coefficient for a damper with a damping gap of 0.15 mm across varying axial lengths. It is observed that the damping coefficient value of c1L3 surpasses that of c1L1 and c1L2 dampers, with minimal peak-to-peak variation. Similarly, Fig. 3(b) depicts the damping coefficient variation for a damper with a damping gap of 0.25 mm and varying axial lengths. The damping coefficient of c2L3 is higher than that of c2L1 and c2L2 dampers, showing minimal peak-to-peak variation. Likewise, Fig. 3(c) demonstrates the damping coefficient for a damper with a damping gap of 0.3 mm and varying axial lengths. Here, the damping coefficient value of c3L3 exceeds that of c3L1 and c3L2 dampers. The observed increase in the damping coefficient with the axial length of the damper can be explained by several underlying factors. Firstly, the longer axial length offers a greater volume for damping, enabling more efficient dissipation of energy from rotor vibrations. Moreover, the extended length encourages improved fluid flow dynamics within the damper, thereby enhancing its overall damping effectiveness. The increased clearance allows for greater movement and flexibility within the damper, potentially resulting in less effective damping of rotor vibrations. Additionally, higher clearance may diminish contact and interaction between the rotor and the damper[20-21], thereby limiting the damping forces exerted on the rotor.

It has been observed that the peak-to-peak variation reduces for higher damping coefficients. In these illustrations, the peak-to-peak variation is depicted to demonstrate the fluctuation in the damping coefficient at a specific location within the CSFD for one complete cycle. Within these plots, “max” denotes the highest values, “mean” signifies the average or mean values, and “min” indicates the lowest values of the parameters being measured. Section 3.2 elaborates on how changes in damping affect the unbalanced response of the test rotor system across different CSFD configurations. The occurrence of a non-circular orbit may result from insufficient damping within the system, which may fail to counteract the applied unbalance adequately. Alternatively, an elliptical orbit could arise due to the asymmetric stiffness of the bearing support. To investigate this phenomenon, the rotor response from the finite element simulation is analysed alongside a frequency spectrum plot.

Table 1. DOE for FE simulation of CSFD

Damping gap (c) (mm)	Axial length (L) (mm)	Case	Figure
0.15	5	c1L1	Fig. 4(a)
0.15	10	c1L2	Fig. 4(a)
0.15	15	c1L3	Fig. 4(a)
0.25	5	c2L1	Fig. 4(b)
0.25	10	c2L2	Fig. 4(b)
0.25	15	c2L3	Fig. 4(b)
0.3	5	c3L1	Fig. 4(c)
0.3	10	c3L2	Fig. 4(c)
0.3	15	c3L3	Fig. 4(c)

3.2 Parametric Study of Nonlinear Response of CSFD

The analysis of different CSFD configurations outlined in Table 1 has been conducted using data from finite element simulations. The variations in parameters affecting the shape and size of each configuration were examined, along with a frequency spectrum analysis to assess CSFD behaviour.

Figure 4 depicts the response of c1L1, c1L2, and c1L3 configurations. The orbits obtained from simulation data for these configurations are shown in Fig. 4(a). Notably, the c1L3 damper displays the smallest circular-shaped orbit, while the c1L1 configuration exhibits the largest non-circular orbit. Figure 4(b) illustrates the frequency spectrum of c1L1 and c1L3, revealing the dominance of the 1X frequency component

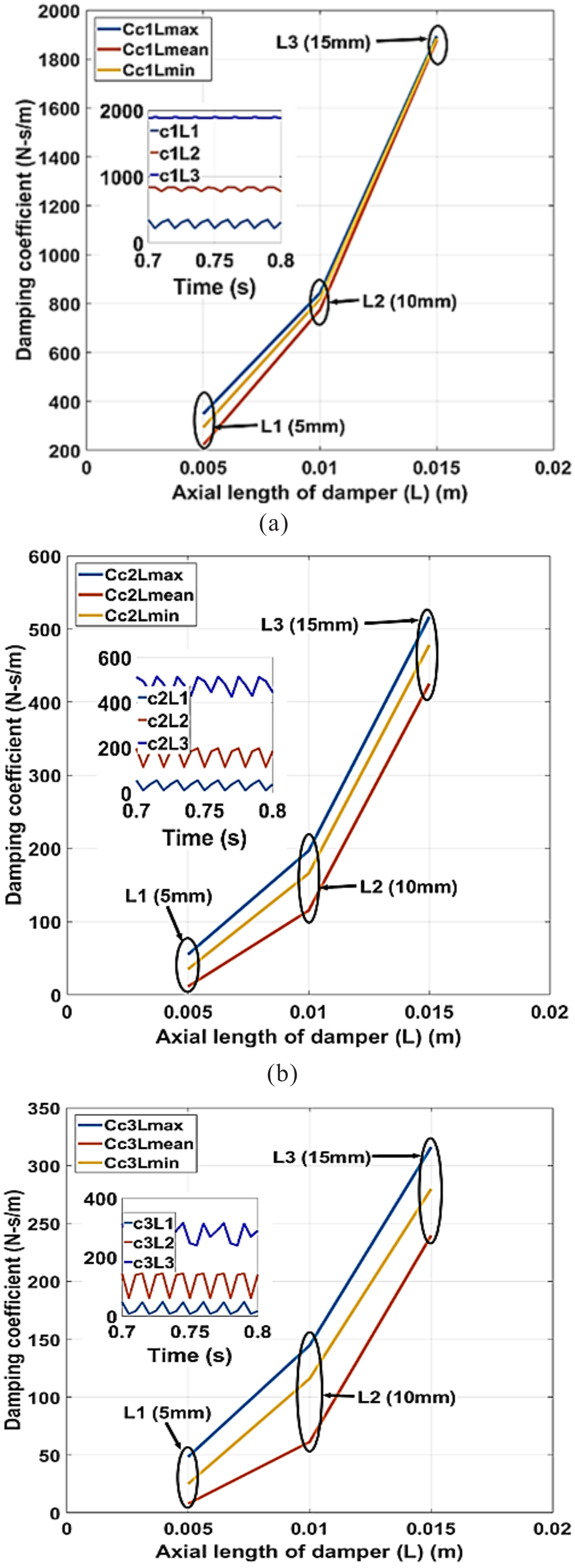

Figure 3. (a) Damping coefficient variation with axial length keeping c1 constant, (b) Damping coefficient variation with axial length keeping c2 constant, and (c) Damping coefficient variation with axial length keeping c3 constant.

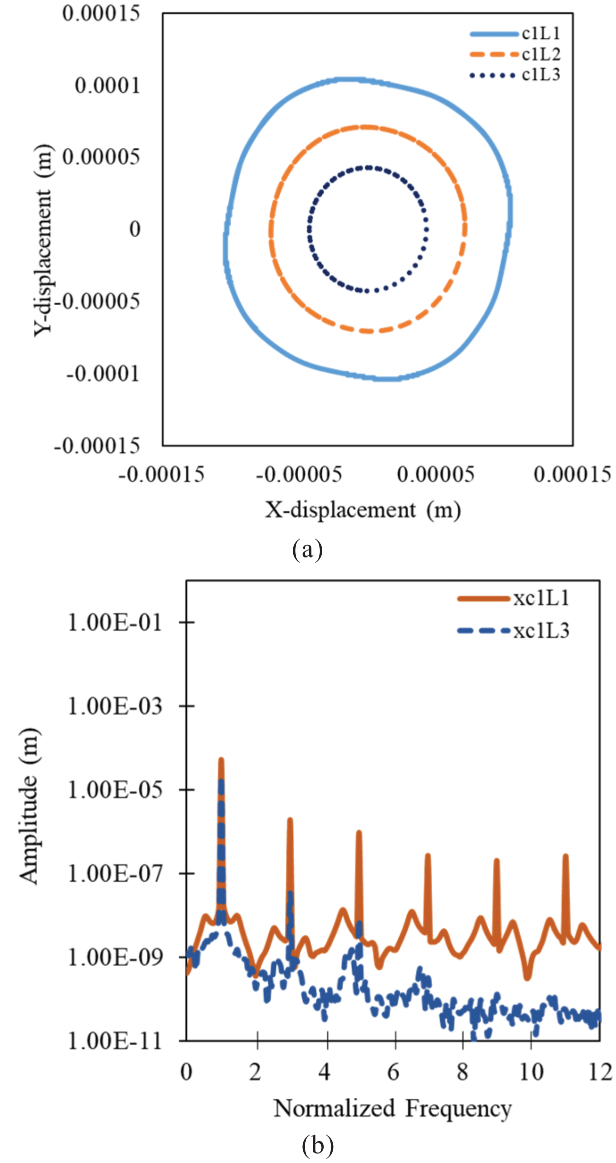

Figure 4. (a) Comparison of unfiltered orbit, and (b) Frequency spectrum of x-direction.

in both cases. However, the frequency spectrum of c1L1 also reveals the presence of higher harmonics (3X, 5X, 7X, 9X, and 11X), indicating nonlinearity within the system.

Figure 5 showcases the response of c2L1, c2L2, and c2L3 configurations. The orbits derived from simulation results for these configurations are non-circular. Notably, the orbit of c2L1 appears highly distorted, while c2L3 exhibits the least distortion. A comparison of Fig. 4(a) and Fig. 5(a) demonstrates that all c2 clearance orbits are larger than c1 clearance orbits due to higher damping in the smaller clearance (c1). Furthermore, in Fig. 5(b), the frequency spectrum of c2L1 and c2L3 reveals the dominant 1X frequency component alongside higher harmonics, suggesting nonlinear behaviour.

Figure 6 illustrates CSFD configurations c3L1, c3L2, and c3L3. The simulation orbits for all three configurations are non-circular (Fig. 6(a)). In Fig. 6(b), the frequency spectrum analysis of the x-direction for c3L1 and c3L3 showcases the presence of both 1X and higher-order (3X, 5X, 7X, 9X,

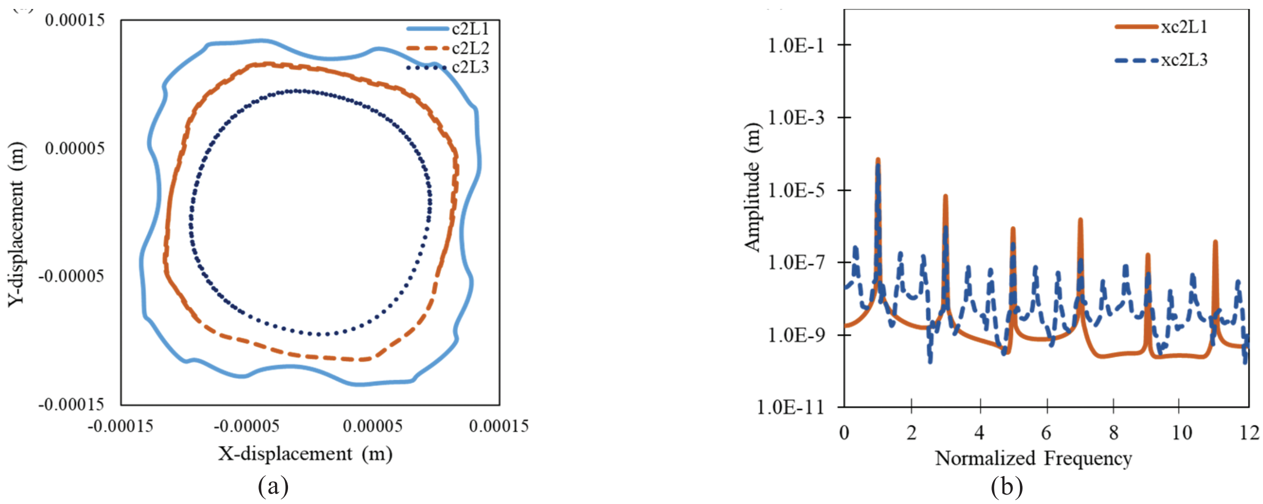

Figure 5. (a) Comparison of unfiltered orbit, (b) Frequency spectrum of x-direction.

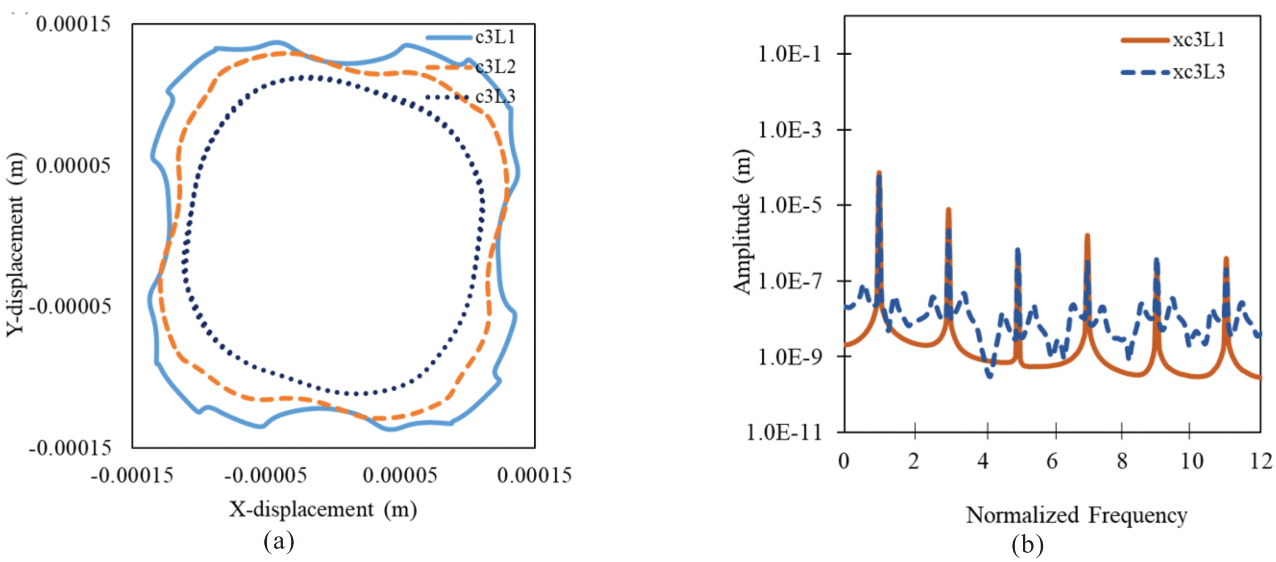

Figure 6. (a) Comparison of unfiltered orbit, and (b) Frequency spectrum of x-direction.

and 11X) frequency components, indicating significant nonlinearity. Additionally, the orbit size for c3 clearance is larger than that for c1 clearance across all specified lengths of CSFD. Given that the damping coefficient of c1 clearance is higher than that of c3 clearance, c3 clearance exhibits less effectiveness in reducing vibration amplitude. The analysis of various CSFD configurations sheds light on their performance characteristics, revealing insights into their behaviour under different conditions. One notable observation is the relationship between damping coefficient variations and the axial length of the damper. This trend, observed across different configurations, underscores the importance of damper length in influencing damping effectiveness. Longer axial lengths provide a larger volume for damping, allowing for more efficient energy dissipation from rotor vibrations. Additionally, the extended length promotes improved fluid flow dynamics within the damper, contributing to enhanced damping efficiency.

Furthermore, the presence of oil in the CSFD introduces additional damping mechanisms, leading to smaller orbit sizes and more effective dampening of rotor vibrations. This finding underscores the significance of fluid properties in influencing CSFD performance. The oil-filled CSFD not only dampens rotor vibrations more effectively but also provides better support and stability to the rotor, resulting in reduced vibration amplitudes. Moreover, the frequency spectrum analysis reveals the presence of nonlinear behaviour within the CSFD system. The dominance of higher harmonics alongside the 1X frequency component suggests complex dynamics at play, which may arise from factors such as asymmetries in stiffness and damping within the system. Understanding these nonlinear effects is crucial for accurately predicting and mitigating rotor vibrations in practical applications. The aforementioned observation can be analysed in light of previously published findings[22-24], indicating that nonlinear damping is pivotal in numerous dynamic systems and can profoundly affect their behaviour and performance.

One important aspect of nonlinear damping is its ability to provide damping forces that vary with the amplitude or velocity of motion. This can lead to complex dynamic behaviours such as frequency-dependent damping, amplitude-dependent damping, and hysteresis effects. Understanding and properly modelling nonlinear damping are essential for accurately

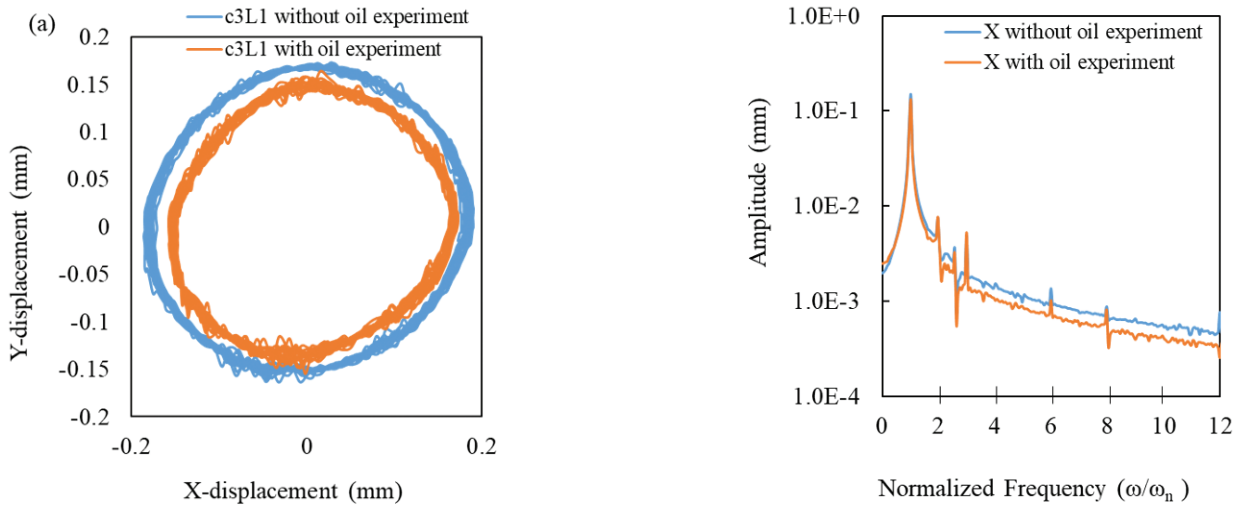

(a) (b)

Figure 7. (a) Comparison of between without and with oil-filled CSFD, and (b) Comparison of x-direction frequency spectrum between without and with oil-filled CSFD.

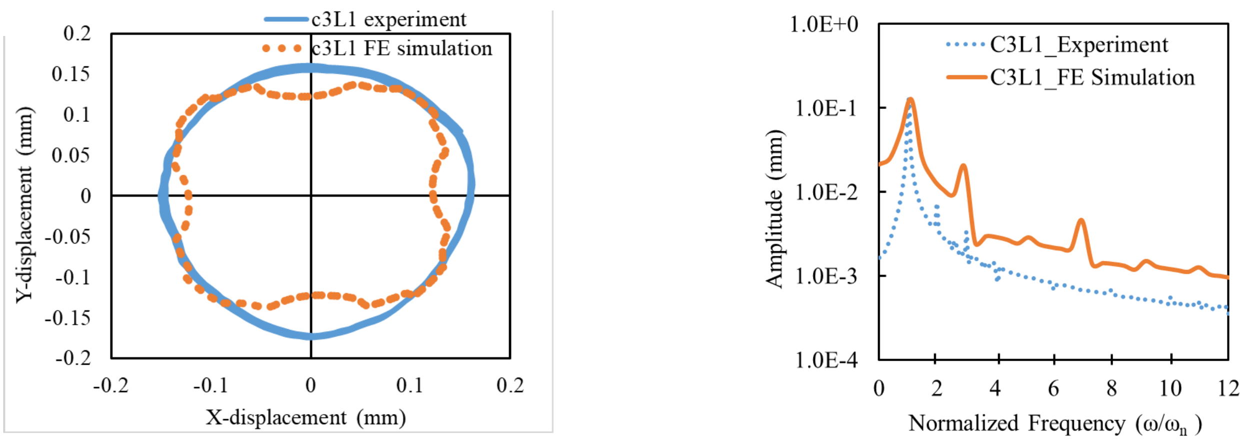

(a) (b)

Figure 8. (a) Comparison of FE simulation and experimental orbit, and (b) Comparison between experimental simulated frequency spectrum of x-direction.

predicting the response of dynamic systems under varying conditions. Additionally, nonlinear damping can help mitigate resonance and stabilize systems by providing damping forces that increase with increasing amplitudes of motion. This can prevent excessive vibration amplitudes and improve system stability, particularly in situations where linear damping alone may be insufficient. Furthermore, nonlinear damping can introduce interesting and beneficial dynamic phenomena such as energy dissipation, frequency tuning, and mode coupling, which can be exploited for vibration control and system optimization.

3.3 Comparison of Experimental Orbit

The experimental setup described in section 2.3, supported by a c3L1 damper, was operated at 1000 rpm with a rotating unbalance mass-eccentricity of 900 gm-mm. The experiment was conducted under both oil-filled and non-oil-filled conditions on the CSFD-supported rotor. The orbits plotted for both scenarios are depicted in Fig. 7(a). It is observed that the orbit size for the oil-filled CFSD-supported rotor is smaller compared to that of the non-oil-filled CFSD-supported rotor. The frequency spectrum shown in Fig. 7(b) reveals only a dominant 1X frequency component for the conducted experiment. The reduction in orbit size for oil-filled CSFD-supported rotors can be attributed to various factors. Firstly, the presence of oil in the CSFD introduces additional damping mechanisms, effectively dampening rotor vibrations and resulting in smaller orbit sizes. Furthermore, the oil-filled CSFD may offer better support and stability to the rotor, reducing the amplitude of its vibrations and consequently leading to smaller orbit sizes.

3.4 Comparison of Experimental and FEM Orbit

This section examines the comparison between experimental and FEM results. Figure 8 displays the orbit and frequency spectrum plots for both sets of data. The vibration amplitudes depicted in Fig. 8(a), orbit plot, and 8(b), frequency spectrum plot, are nearly identical for both experimental and FEM results. However, despite applying the same rotating unbalance force, the experimental results exhibit slightly less nonlinear behaviour compared to the FEM simulation. This difference can be attributed to the linear nature of the integral spring stiffness, which effectively captures minor nonlinearities induced by high unbalance and fluid presence. In contrast, the FE simulation incorporates a nonlinear fluid element, resulting in the presence of odd nonlinear frequency components[25] in the frequency spectrum, particularly due to the high unbalance in the system. The non-circular orbit observed in the FE simulation is primarily caused by the significant presence of the 3X nonlinear frequency component in the frequency spectrum.

3.5 Response Plot of Test Rotor Supported on CSFD

A coast-up experiment was conducted on the test rig described in section 2.3 to evaluate the effectiveness of CSFD while the rotor traverses its critical speed. The experiment was conducted using test rigs supported by c3L1 and c3L3 dampers. Figure 9(a) illustrates the vertical response of the rotor supported by the c3L1 damper, indicating a weak control of vibration amplitude as the critical speed is approached. Similarly, Figure 9(b) displays the response plot of the rotor supported by the c3L3 damper, showing a significant reduction in vibration amplitude as the critical speed is traversed.

These observations suggest that the oil-filled c3L3 damper is more effective than the c3L1 damper, aligning with the higher damping coefficient value of the c3L3 damper indicated in section 3.1. These response plots exhibit similar trends to those reported by Bonello[7], *et al.*, with a sharp rise in response approaching the critical speed and a gradual drop as the speed moves away from the critical, indicating the presence of softening nonlinearity in the system. This observation is further supported by the results obtained in sections 3.2 and 3.3, where the frequency spectrum for c3L1 and c3L3 reveals the presence of odd harmonics, indicating nonlinear behaviour. Additionally, the damping ratios for c3L1 and c3L3 dampers, calculated from the quality factor, are 0.0681 and 0.11, respectively, suggesting almost twice the damping ratio in c3L3 compared to c3L1.

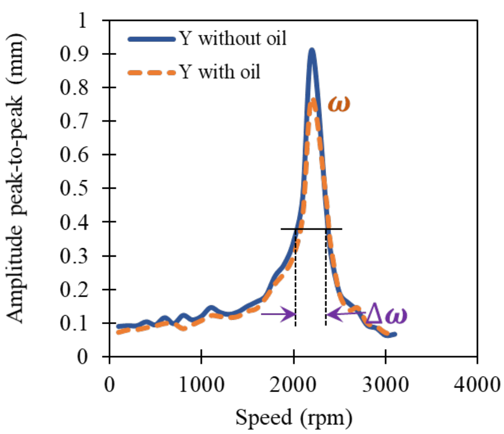

(a)

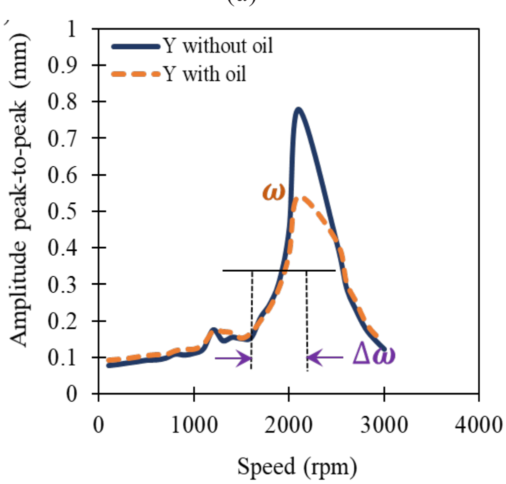

(b)

Figure 9. (a) Horizontal direction response of 5 mm CSFD (c3L1), and (b) Vertical direction response of 5mm CSFD (c3L3).

4. COMPARISON OF MODIFIED RAYLEIGH OSCILLATOR WITH PROPOSED CSFD

As evident from the orbits and frequency spectrum of the proposed CSFD, it's notable that the orbits deviate from circularity, possibly indicating the presence of nonlinear damping, as discussed in section 3.5. With an increase in the damper length, higher damping coefficients are observed, leading to progressively circular orbits. Through a modified Rayleigh Oscillator equation, we investigated the interaction between nonlinear and linear damping, aiming to elucidate the role of nonlinear damping in rotor systems and its correlation with the behaviour of CSFD nonlinear damping.

The equation of the modified Rayleigh Oscillator is given by:

$$\begin{aligned}&\ddot{x} + \omega_1^2 x + b(1+c\dot{x}^2)\dot{x} - \gamma\omega_1^2 y = F_o \cos\omega t\\&\ddot{y} + \omega_2^2 y + b(1+c\dot{y}^2)\dot{y} + \gamma\omega_2^2 x = F_o \sin\omega t\end{aligned} \qquad (1)$$

This model incorporates both linear and cubic damping components. The presence of the cubic damping component is observed to produce odd frequency components, as depicted in the finite element result figures 4, 5, and 6. To examine the parametric influence, the model is non-dimensionalised in Eqn. (2).

$$\begin{aligned}&\ddot{x} + \varpi_1^2 x + 2\varsigma\varpi_1(1+\delta\dot{x}^2)\dot{x} - \gamma\varpi_1^2 y = \varpi^2\cos\varpi\tau\\&\ddot{y} + \varpi_2^2 y + 2\varsigma\varpi_2(1+\delta\dot{y}^2)\dot{y} + \gamma\varpi_2^2 x = \varpi^2\sin\varpi\tau\end{aligned} \qquad (2)$$

Where, $\varpi_1 = \omega_1/\Omega$, $\varsigma = b/2m\omega_1$, $\delta = ce^2/b$, $\varpi = \omega/\Omega$, $\tau = \Omega t$

The values of parameters for our proposed CSFD and damping coefficient as obtained through experiment and simulation are listed in Table 2.

Table 2. Parameter used in solving modified Rayleigh oscillator equation

ω_1	167 Hz
ς	0.05
γ	0.1
δ	0.5, 5, 50
ω	16.67 HZ

The modified Rayleigh's oscillator equation has been solved using the 4th-order Runge-Kutta method. The step size chosen is 1e-03. One million data points have been generated, and numerical transient has been removed.

The value of the nonlinear damping coefficient has varied, as listed in the table, and changes in orbit shape and frequency

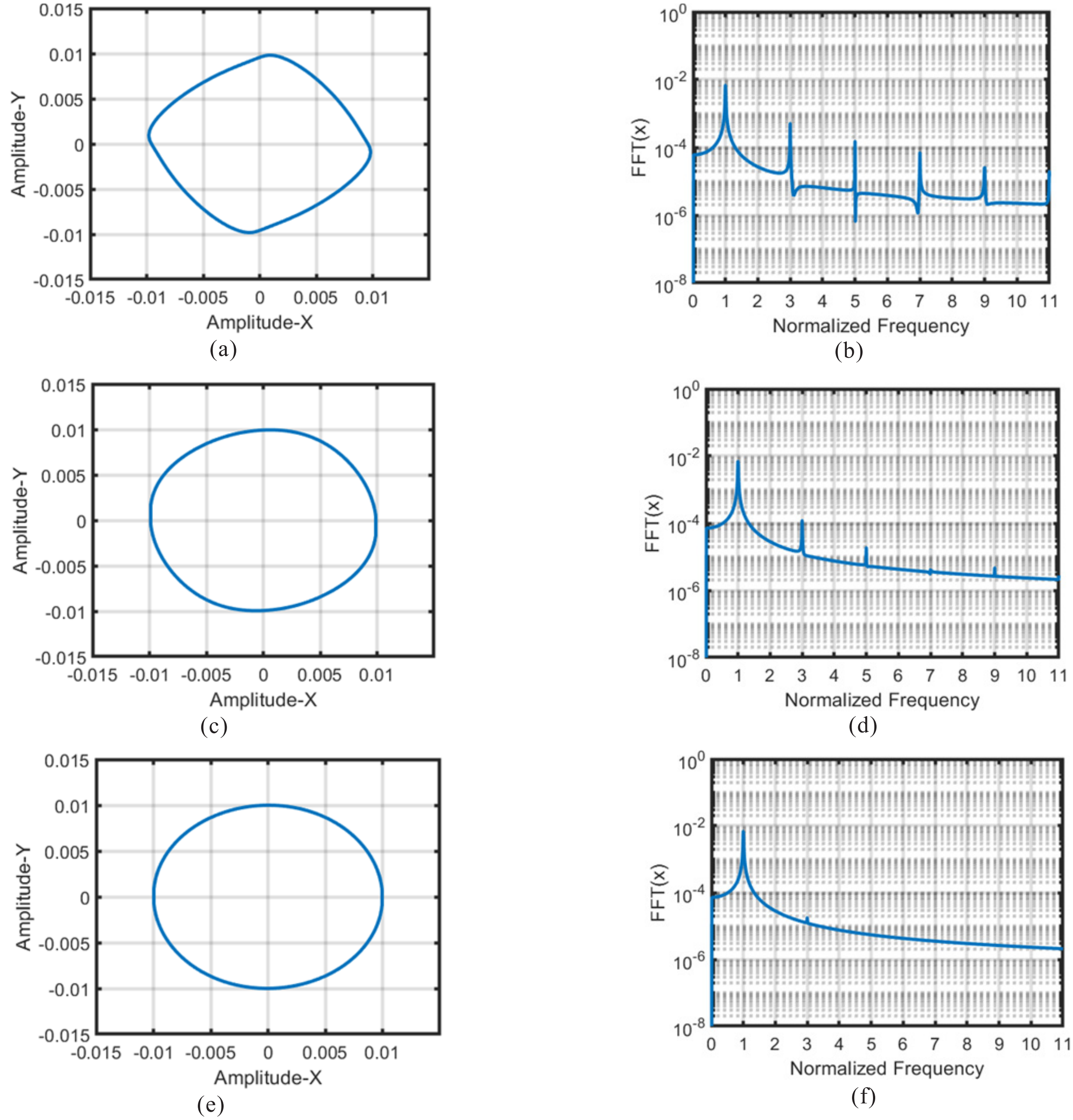

Figure 10. (a) Orbit at δ=50, (b) Frequency Spectra at δ=50, (c) Orbit at δ=5, (d) Frequency Spectra at δ=5, (e) Orbit at δ =1, and (f) Frequency Spectra at δ=1.

spectra have been observed. Figure 9 shows the orbits and the frequency spectra of the modified Rayleigh oscillator.

The following observation can be made from the results obtained by simulating Modified Rayleigh's oscillator with parameters of CSFD:

- When the value δ is 50, which contributes to the nonlinear damping very high, the shape of the orbit is almost rectangular (Figure 10(a)). When the value δ decreases from 50 to 5, the orbit shifts towards a circular shape. A correlation can be drawn between Figures 4,5 and 6 of CSFD and Fig. 10 of Rayleigh's Oscillator, where the shape shifts from rectangular to circular with a change in damping value.
- Though Rayleigh's Oscillator does not pitch the exact mathematical model for the proposed CSFD, the similarity between the two is significant. This hint is to investigate and modify Rayleigh's Oscillator further to bring out the correct model for CSFD in future work.

5. CONCLUSIONS

In the present study, a CSFD has been designed and manufactured, which is essentially a compact SFD with retainer/centralizing springs. The FE simulation and experiment were performed on the proposed CSFD model using different parameters. An analytically modified model of the Rayleigh oscillator has been used to understand the effect of linear and nonlinear damping. The following can be concluded about the proposed CSFD:

The CSFD offers more damping as we increase the axial length (L), keeping the damping gap (c) constant, which is per the Reynolds Equation. The damping coefficient of the CSFD varies periodically, as shown in Fig. 3. Maximum damping is offered for the c1L3 configuration of the damper, as observed in Fig. 3(a).

The orbit plot in Fig. 4(a) shows that the orbit of the c1L3 configuration is almost circular. This implies that this configuration of CSFD is effective in reducing the contribution of higher harmonics in the vibration of the rotor.

The damping ratio obtained from the experimental response plot is 0.11 for the c3L3 case. Spring softening can be observed in CSFD for the c3L3 configuration but not in CSFD for the C3L1 configuration, as shown in Fig. 9. This implies that the increased length of CSFD not only affects the damping of the system but also plays a vital part in the spring softening of the rotor.

The modified Rayleigh oscillator studied in section 4 hints towards the presence of cubic nonlinear damping in the proposed CSFD design. The frequency spectra of the oscillator in Fig. 10 have similar harmonics as can be observed in CSFD spectra, which are 3x, 5x, and so on.

REFERENCES

1. Adiletta, G. & Della Pietra, L. The squeeze film damper over four decades of investigations. Part II: Rotordynamic analyses with rigid and flexible rotors. *The Shock and Vibration Digest*, 2002, **34**(2), 97-126.
2. Agnew, J. & Childs, D. Rotordynamic characteristics of a flexure pivot pad bearing with an active and locked integral squeeze film damper. In Turbo Expo 2012: Power for Land, Sea, and Air, American Society of Mechanical Engineers., 2012, 44731, 551-561. doi:10.1115/GT2012-68564
3. Andrés, L.S. & Lubell, D. Imbalance response of a rotor supported on open-ends Integral squeeze film dampers. Proceedings of the ASME Turbo Expo, 1998. doi:10.1115/97-GT-012
4. Bao, M.; Yang, H.; Sun, Y. & French, P.J. Modified Reynolds' equation and analytical analysis of squeeze-film air damping of perforated structures. *J. Micromech. Microengin.*, 2003, **13**(6), 795–800. doi:10.1088/0960-1317/13/6/301
5. Bonello, P.; Brennan, M.J. & Holmes, R. Nonlinear modelling of rotor dynamic systems with squeeze film dampers - An efficient integrated approach. *J. Sound and Vibration*, 2002, **249**(4), 743–773. doi:10.1006/jsvi.2001.3911
6. Chen, P.Y.P. & Hahn, E.J. Side clearance effects on squeeze film damper performance. *Tribology Int.*, 2000, **33**(3-4), 161–165. doi:10.1016/S0301-679X(00)00022-0
7. Chu, F. & Holmes, R. Efficient computation on nonlinear responses of a rotating assembly incorporating the squeeze-film damper. Comput. *Methods in Appl. Mech. Engin.*, 1998, **164**(3-4), 363–373. doi:10.1016/S0045-7825(98)00097-8
8. De Santiago, O. & Andrés, L.S. Dynamic response of a rotor-integral squeeze film damper to couple imbalances. Proceedings of the ASME Turbo Expo, 2000, **4**. doi:10.1115/2000-GT-0388
9. De Santiago, O.C. & San Andrés, L.A. Imbalance response and damping force coefficients of a rotor supported on end sealed integral squeeze film dampers. Proceedings of the ASME Turbo Expo, 1999, **4**(1985), 6-11. doi:10.1115/99-GT-203
10. Yakoub, R.Y. & El-Shafei, A. A fast method to obtain the nonlinear response of multi-mode rotors supported on squeeze film dampers using planar modes: Part II -Parametric studies. Proceedings of the ASME 1998 International Gas Turbine and Aeroengine Congress and Exhibition. doi:10.1115/98-GT-413
11. Ertas, B.; Cerny, V.; Kim, J. & Polreich, V. Stabilizing a 46 MW multistage utility steam turbine using integral squeeze film bearing support dampers. *J. Engin. Gas Turbines and Power*, 2015, **137**(5), 1–11. doi:10.1115/1.4028715
12. Ertas, B.; Delgado, A. & Moore, J. Dynamic characterization of an integral squeeze film bearing support damper for a supercritical Co2 expander. *J. Engin. Gas Turbines and Power*, 2018, **140**(5), 1–9. doi:10.1115/1.4038121
13. Locke, S.R. & Faller, W. Recycle gas compressor designed for high unbalance tolerance and stability. Proceedings of the 32nd Turbomachinery Symposium, 2003. Texas A&M University. Turbomachinery Laboratories.
14. Lu, X.; Andrés, L.S.; Koo, B. & Tran, S. On the effect of the gap of end seals on force coefficients of a test integral squeeze film damper: Experiments and predictions. *J. Engine. Gas Turbines and Power*, 2021, **143**(1), 1–14. doi:10.1115/1.4048700
15. San Andrés, L. & De Santiago, O. Imbalance response of a rotor supported on flexure pivot tilting pad journal bearings in series with integral squeeze film dampers. *J. Engine. Gas Turbines and Power*, 2003, **125**(4), 1026–1032. doi:10.1115/1.1492831
16. Xing, C.; Braun, M.J. & Li, H. A three-dimensional navier-stokes-based numerical model for squeeze film dampers. Part 2- Effects of gaseous cavitation on the behaviour of the squeeze film damper. *Tribol. Transact.*, 2009, **52**(5a), 695–705. doi:10.1080/10402000902913311
17. Xing, C.; Braun, M.J. & Li, H. A three-dimensional navier-stokes–based numerical model for squeeze-film dampers. Part 1: Effects of gaseous cavitation on pressure distribution and damping coefficients without consideration of inertia. *Tribol. Transact.*, 2009, **52**(5b), 680–694. doi:10.1080/10402000902913303
18. Yakoub, R.Y. & El-Shafei, A. A fast method to obtain the nonlinear response of multi-mode rotors supported on squeeze film dampers using planar modes: Part I: Theory. In Turbo Expo 1998: Power for Land, Sea, and Air, ASME, 1998. doi:10.1115/98-GT-412
19. Zeidan, F.Y.; San Andres, L. & Vance, J.M. Design and

application of squeeze film dampers in rotating machinery. Proceedings of the Twenty-Fifth Turbomachinery Symposium, 1996. Texas A&M University. Turbomachinery Laboratories.
doi:10.21423/R1694R

20. Barabas, S.; Florescu, A. & Sarbu, F. Study of hydrodynamic behaviour of large bearings depending on the viscosity of the lubricant. *In* MATEC Web of Conferences, 2017, **121**, PP. 03003.
doi: 10.1051/matecconf/201712103003MSE 2017
21. Kong, F.; Huang, W.; Jiang, Y.; Wang, W. & Zhao, X. Research on the effect of damping variation on vibration response of defective bearings. *Adv. Mech. Engine.*, 2019 **11**(3), 1687814019827733.
doi: 10.1177/1687814019827733
22. Yang, Y.; Chen, G.; Ouyang, H.; Yang, Y. & Cao, D. Nonlinear vibration mitigation of a rotor-casing system subjected to imbalance–looseness–rub coupled fault. *Int. J. Nonlinear Mech*, 2020, **122**, 103467.
doi:10.1016/j.ijnonlinmec.2020.103467
23. Gourdon, E.; Alexander, N.A.; Taylor, C.A.; Lamarque, C.H. & Pernot, S. Nonlinear energy pumping under transient forcing with strongly nonlinear coupling: Theoretical and experimental results. *J. Sound and Vibration*, 2007, **300**(3-5), 522-551.
doi:10.1016/j.jsv.2006.06.074
24. Sigalov, G.; Gendelman, O.V.; Al-Shudeifat, M.A.; Manevitch, L.I.; Vakakis, A.F. & Bergman, L.A. Resonance capture and targeted energy transfers in an inertially-coupled rotational nonlinear energy sink. Nonlinear dynamics, 2012, **69**, 1693-1704.
doi:10.1007/s11071-012-0379-1
25. Goldman, P. & Muszynska, A. Application of full spectrum to rotating machinery diagnostics, 1999. (Doctoral dissertation, Bently Rotor Dynamics Research Corporation).

CONTRIBUTORS

Mr Anurag Kumar obtained his M Tech (Mechanical Engineering, Machine Design) from National Institute of Technology Calicut. His areas of research include: Squeeze film damper and non-linear dynamics.
In the current study, he designed and fabricated the compact squeeze film damper (CSFD) using Wire-EDM which has been used for analytical study and to perform experimentation in this manuscript and has prepared the manuscript.

Mr Aman K. Srivastava obtained his BTech (Mechanical Engineering) from IIT, Patna. His areas of interest include: Non-linear dynamics.
In the current study, he helped in performing experimentation and have done validation of results with nonlinear model of Rayleigh Oscillator and has prepared the manuscript.

Prof. (Dr) Mayank Tiwari obtained his PhD from IIT, Delhi and further did Post Doctorate from Ohio State University. He is working as a Professor in the Department of Mechanical Engineering at IIT Patna. His area of interests are rotor dynamics, gas turbine engines, friction wear, lubrication.
In the current study, he provided ideas and guidance which has led to the layout of the work presented in the paper and has carried out the review process of manuscript.

Dr Akhilendra Singh obtained his PhD from BITS, Pilani Rajasthan. Currently working as an Associate Professor in the Department of Mechanical Engineering at IIT Patna. His area of interests are FEM, XFEM, meshfree method, computational mechanics, fracture and fatigue, thermal engineering, etc.
In the current study, he provided ideas and guidance which has led to the layout of the work presented in the paper and has carried out the review process of manuscript.